












Conferências Plenárias

CPI1

CORROSION BEHAVIOUR OF Fe- AND Ni-BASED ALLOYS IN SOLAR SALT AND CORROSION MITIGATION STRATEGIES VIA PROTECTIVE COATINGS

Ceyhun Oskay^{1*} ; T. M. Meissner¹ ; B. Grégoire² ; B. O. Burek¹ ; C. Schlereth¹ ; A. Bonk³ ; M. Bik⁴ ; A. Solimani¹ ; M.C. Galetz¹ 

¹ DEHEMA-Forschungsinstitut, Frankfurt (Main), Germany, ceyhun.oskay@dechema.de

² Birmingham Centre for Energy Storage (BCES), University of Birmingham, Birmingham, United Kingdom

³ German Aerospace Center (DLR), Stuttgart, Germany

⁴ AGH University of Science and Technology, Krakow, Poland

* Corresponding author

<https://doi.org/10.34637/3jh1-ab40>

ABSTRACT

This study investigated the corrosion behaviour of commercial and model Fe- and Ni-based alloys in solar salt at 600°C. The thermal decomposition of nitrate salts led to an increasing concentration of oxidizing agents in the salt melt and thus to a higher corrosion rate. For Fe-based alloys, the oxide scales contained a Na- and Fe-rich outer layer, followed by an inner Cr-rich layer and nitridation as well as Cr-depletion was observed at the scale/metal interface. Furthermore, higher extent of chloride impurities in solar salt, led to a significantly higher corrosion rate for ferritic-martensitic alloys. For Ni-based alloys, the formation of a duplex scale consisting of a NiO outer and Ni-Cr spinel layer showed protective character during isothermal exposure; however even for Ni-based alloys, Cr was detected in the salt melt, which showed evidence for its dissolution in the melt as toxic hexavalent Cr. Diffusion aluminide and electroless Ni-P coatings deposited on cost-efficient ferritic-martensitic alloys led to formation of protective oxide scales and hindered the Cr-dissolution into the salt melt.

Keywords: Concentrated solar power, Molten nitrate corrosion, Cr-dissolution, Protective coatings

1. INTRODUCTION

The utilization of thermal energy storage (TES) systems in solar power plants has increased the competitiveness of the concentrated solar power (CSP) technology among other renewable energy generation methods. Molten nitrate salts, particularly the mixture of 60 wt.% NaNO₃ and 40 wt.% KNO₃ (also known as “solar salt”), are used as a state-of-the-art heat transfer fluid (HTF) in solar power tower systems. While offering beneficial thermal and physical properties such as high heat capacity, low viscosity, and low melting point [1], their application as HTF leads to significantly high corrosion rates for components. This limits the material selection to austenitic alloys as structural materials in CSP plants [2], whereas the insufficient corrosion resistance hinders the use of cost-effective ferritic-martensitic (FM) steels [3]. In this study, the prevailing corrosion mechanisms for commercial and model Fe- and Ni-based alloys immersed in molten nitrate salts are investigated. Furthermore, based on the findings for the alloys, corrosion mitigation strategies via protective coatings are developed, and their applicability for the CSP technology are evaluated.

2. DESCRIPTION

Coupon samples (20x10x2 mm³) of FM steels P91 and X20CrMoV12-1 (hereafter named as X20), austenitic steel Alloy 800H, commercial Ni-based alloys Haynes-230 (hereafter named as Alloy 230), Alloy 617B, Alloy 602 CA and two model Ni-based alloys with varying Fe, Cr and Al-contents (NiCr25Al3Fe9 and NiCr30Al2.8Fe0.6), were machined using wire-cutting. The samples were glass-bead blasted and degreased in ultrasonic ethanol bath. Two different coatings were applied on FM steels. Diffusion aluminide coatings were deposited on P91 by pack cementation at 1000°C, while electroless deposition was used to manufacture Ni-P coatings on X20 steel. Solar salt mixture was prepared by mixing technical grade NaNO₃ and KNO₃ (60-40 wt.%, Salt A). In order to investigate the influence of chloride impurities on the corrosion behaviour of alloys in solar salt, two different salt mixtures were also prepared by increasing the chloride impurity extent to 500 ppm (Salt B) and 1000 ppm (Salt C). Isothermal static immersion tests in the aforementioned three different solar salt mixtures with varying chloride content were conducted inside alumina crucibles, placed in a quartz-tube furnace under flowing (4L/h) synthetic air at 600°C up to a maximum duration of 1000 h. Salt C samples with the highest impurity content were analyzed after 1000 h immersion of different alloys by an inductively coupled plasma mass spectrometer (ICP-MS) to quantify the Cr-leaching from the alloys into the salt melt. After the fully immersed salt exposure, coated and uncoated alloy samples were rinsed in warm distilled water to remove the salt remnants followed by the determination of the specific net mass change using a precision weighing balance. Thereafter, cross-sections were prepared using conventional metallographic methods. X-ray diffraction (XRD), Raman-spectroscopy, scanning electron microscopy (SEM) and electron-probe microanalysis (EPMA) were utilized to characterize the corrosion products as well as the compositional and microstructural changes in the sub-surface of alloys as well as coatings.

3. RESULTS AND DISCUSSION

Figure 1 shows the specific net mass change kinetics of X20, Alloy 800H and Alloy 230 during isothermal immersion in molten solar salt with varying chloride content at 600°C. The onset of breakaway corrosion for X20 alloy is significantly shortened during exposure in impure salts, which can be explained by the formation of volatile chlorides in the alloy's sub-surface zone and their oxidation at the surface with the chlorination-oxidation process also known as "active oxidation". On the other hand, the scaling behavior of austenitic alloys is less sensitive to the impurity content of the solar salt. A linear mass loss is observed for Haynes-230, which is attributed to scale dissolution by fluxing mechanisms outweighing the mass gain by oxidation.

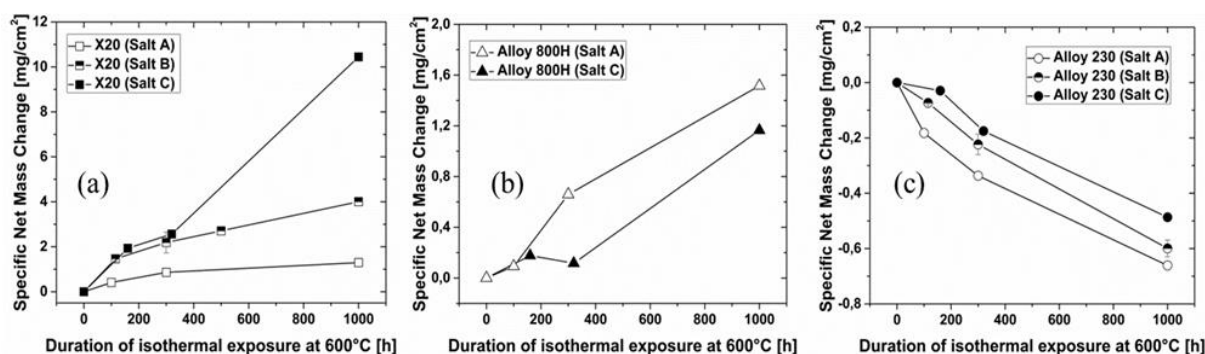


Figure 1 – Specific net mass change kinetics of (a) X20, (b) Alloy 800H and (c) Alloy 230 in solar salt with varying impurity content.

Figure 2 shows the Cr-concentration in different Salt C samples after the exposure of alloys and the calculated specific Cr-loss from the alloys. Cr is dissolved from all tested alloys due to the formation of mono- and dichromates by either basic fluxing mechanisms and/or the reaction of Cr with nitrate anions. Considering the

large salt reservoir of modern CSP plants exceeding several thousand tons, the formation of toxic chromates in the salt can lead to the necessity of laborious salt regeneration, unless the chromate formation is mitigated.

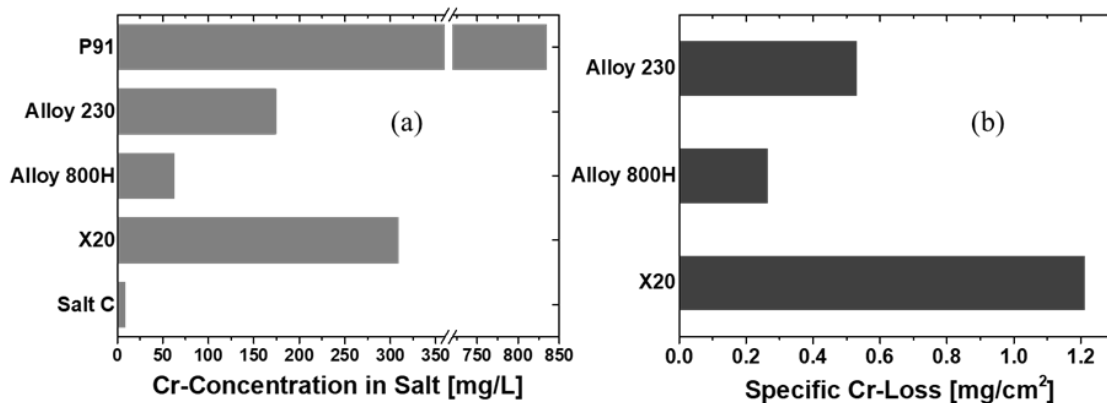


Figure 2 – Cr-concentration in Salt C samples after the immersion of alloys at 600°C for 1000 h shown together with the Cr-concentration in the blank Salt C; (b) specific Cr-loss calculated for different alloys.

Figure 3 illustrates the cross-sectional BSE images and EPMA elemental distribution maps of X20, Alloy 800H and Alloy 230 after 1000 h of immersion in Salt C at 600°C. An almost 75 μm thick and non-protective scale consisting of alternating bands of NaFeO_2 and Fe_2O_3 was formed on X20 (phases confirmed by XRD, not shown here). Underneath the oxide scale, a 25 μm thick nitridation zone was observed, in which Cr was bound within nitride precipitates. Unlike X20, Alloy 800H was able to form a much denser and thinner oxide scale consisting of a NaFeO_2 and hematite outer layer and a Cr-rich spinel inner layer. Underneath the scale, Fe and Cr depletion was observed. The state-of-the-art Alloy 230 forms an almost 10 μm thick scale consisting of an outer NiO and an inner Ni-Cr spinel layer followed by an altered sub-scale zone showing internal oxidation and nitridation as well as Cr-depletion, which is the consequence of the Cr-leaching into the salt melt (see Figure 2.a).

Figure 4 depicts the cross-sectional BSE-micrographs and EPMA elemental distribution maps of the model Ni-based alloys with varying Fe-, Cr- and Al-content. $\text{NiCr}_{25}\text{Al}_3\text{Fe}_9$ formed a very thin and protective Al-rich oxide scale, which effectively reduced the Cr-depletion in the sub-surface of the alloy. On the other hand, despite its higher Cr-content $\text{NiCr}_{30}\text{Al}_{2.8}\text{Fe}_{0.6}$ showed higher Cr-depletion underneath the oxide scale, which contained a Na-rich outer layer followed by a Ni-rich oxide layer and an internal oxidation and nitridation zone. The significant differences between the corrosion behaviours of both model alloys despite their relatively similar chemical composition by means of Cr and Al, can be explained by the differences in the Al-activity at the surface. The Al-activity in $\text{NiCr}_{25}\text{Al}_3\text{Fe}_9$ was roughly three times higher than that of $\text{NiCr}_{30}\text{Al}_{2.8}\text{Fe}_{0.6}$. This can be attributed to the higher Fe-content of the first model alloy compared to the latter one, which results in an increase in the Al-activity thereby leading to the formation of a protective Al-rich oxide scale and effectively hindering the Cr-dissolution to the salt melt.

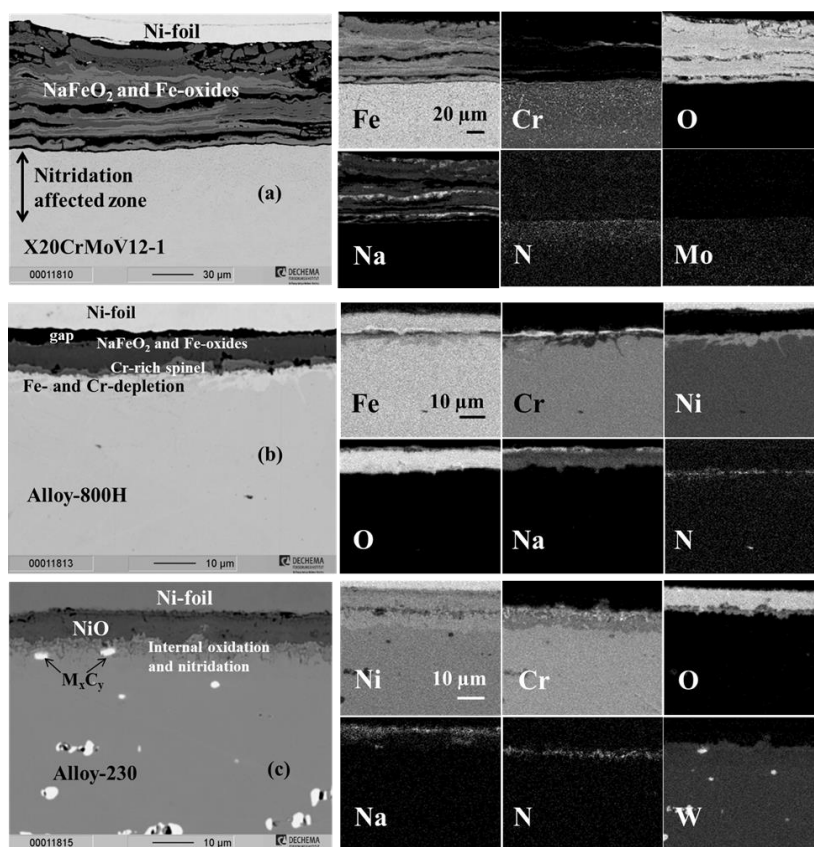


Figure 3 – Cross-sectional BSE images and EPMA elemental distribution maps of (a) X20, (b) Alloy 800H and (c) Alloy 230 after 1000 h immersion in Salt C at 600°C. Please note the varying magnification in respective images.

Based on the obtained results showing a high corrosion resistance for Ni-based alloys in molten solar salt compared to Fe-based alloys and an even further increase in their corrosion resistance with a sufficiently high Al-activity, two coating mitigation strategies were developed for cost-efficient FM steels to enable their applicability in CSP plants as structural materials and to hinder Cr-dissolution into the salt melt: (1) increasing the Ni-content by the electroless deposition of Ni-P coatings; (2) increasing the Al-content by pack cementation.

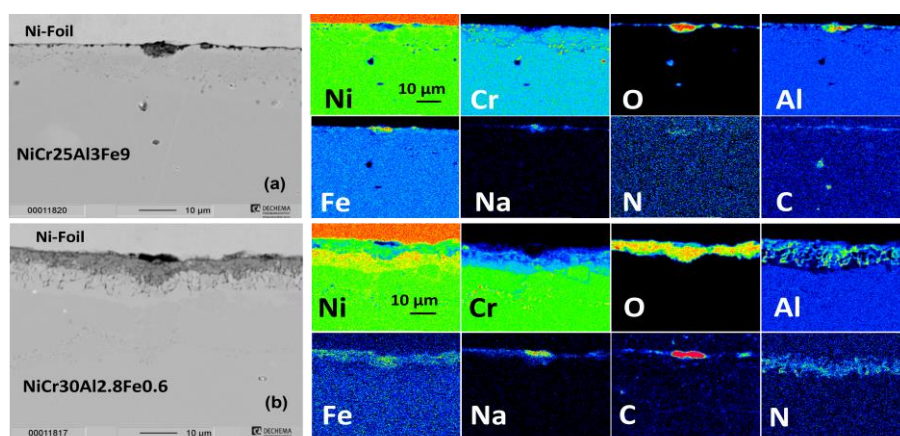


Figure 4 – Cross-sectional BSE images and elemental distribution maps of model Ni-based alloys, (a) NiCr25Al3Fe9 and (b) NiCr30Al2.8Fe0.6 after 1000 h immersion in Salt C at 600°C.

The aluminide coating consisted of an Al-rich outer layer formed by FeAl_2 and Fe_2Al_5 phases followed by a thicker B2-FeAl layer and a ferritic Al-Diffusion zone (see Figure 5.a). After the immersion in Salt A for 1000 h at 600°C , the coating microstructure barely changed (see Figure 5.b). The only oxide phase was the $\alpha\text{-Al}_2\text{O}_3$ (characterized by Raman-spectroscopy) and EPMA line scans showed a slight Na enrichment at the surface of the oxide (not shown). Considering the severe Cr-leaching from uncoated P91 into the salt melt (see Figure 2.a), the corrosion resistance of FM steels can be significantly improved and the leaching of Cr from the alloy can be hindered by aluminide coatings. Ni-P coatings on X20 steel formed a thin oxide scale consisting of NiO and Ni-Fe spinel (see Figure 5.c) Underneath the oxide scale, Ni_3P phase was formed during exposure and acted as a diffusion barrier against Cr outward diffusion. This can be observed by the rare presence of Cr in the coating. Compared to the state-of-the-art Alloy 230 (see Figure 3.c), Ni-P coatings on FM steels formed similar oxide scales and effectively hinder the Cr-dissolution from the alloy to the melt.

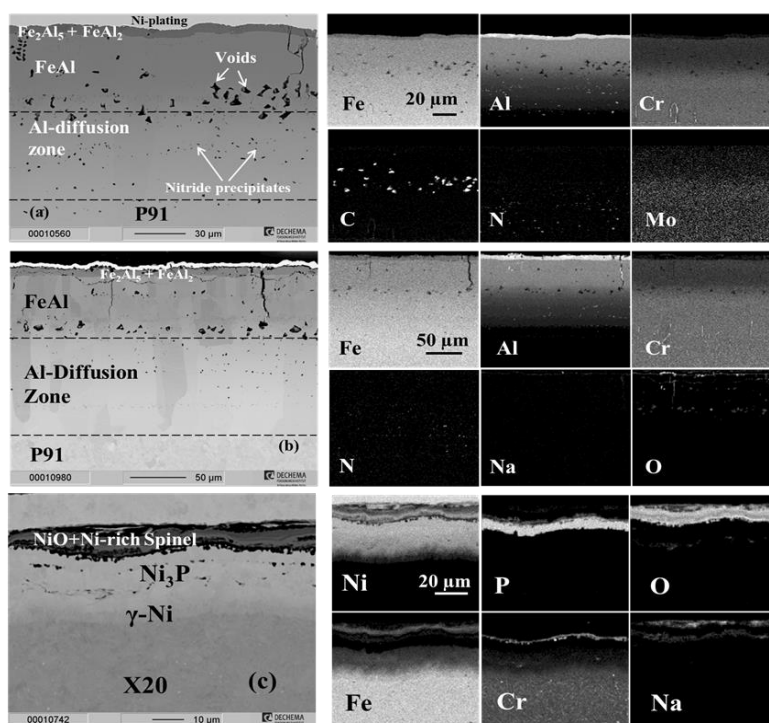


Figure 5 – Cross-sectional BSE images and elemental distribution maps of (a) as-deposited aluminide coating on P91, (b) aluminized P91 and (c) Ni-P coated X20 after 1000 h of immersion in Salt A at 600°C .

4. CONCLUSIONS

The prevailing corrosion mechanisms in molten nitrate salts are the thermal decomposition reactions of nitrate anions resulting in an increase in the concentration oxidizing species in the salt melt and the dissolution of Cr from the alloy into the salt melt. An increase in the chloride content of the solar salt results in significantly higher corrosion rates for FM steels, whereas the austenitic alloys are less sensitive to the impurity levels investigated in this study. While a Ni-rich oxide scale showed protective character for Ni-based alloys, thicker oxide scales formed on Fe-based alloys. The corrosion resistance of Ni-based alloys was increased significantly through the increase of Al-activity in the alloy. The corrosion resistance of FM steels can be significantly improved by either the application of aluminide or Ni-P coatings, which both form protective oxide scales and effectively hinder the dissolution of Cr from the alloy.



ACKNOWLEDGEMENTS

Authors thank European Commission's Horizon 2020 research and innovation project "RAISELIFE" for funding this work under the grant No. 686008. Haynes International Ltd. and VDM Metals Group are gratefully acknowledged for providing nickel alloy materials.

REFERENCES

- [1] A. Bonk, S. Sau, N. Uranga, M. Hernaiz, T. Bauer, Advanced heat transfer fluids for direct molten salt line-focusing CSP plants. *Prog. Energy Combust. Sci.* 67 (2018) 69-87, <https://doi.org/10.1016/j.pecs.2018.02.002>
- [2] M. Walczak, F. Pineda, A.G. Fernández, C. Mata-Torres, R.A. Escobar, Materials corrosion for thermal energy storage systems in concentrated solar power plants. *Renew. Sust. Energ. Rev.* 86 (2018) 22-44, <https://doi.org/10.1016/j.rser.2018.01.010>
- [3] A. Soleimani-Dorcheh, M.C. Galetz, Sol. Slurry aluminizing: A solution for molten nitrate salt corrosion in concentrated solar power plants. *Sol. Energy Mater. Sol. Cells* 146 (2016) 8-15, <https://doi.org/10.1016/j.solmat.2015.11.024>